Biosensors and Bioelectronics 25 (2009) 820–825

Contents lists available at ScienceDirect

Biosensors and Bioelectronics

journal homepage: www.elsevier.com/locate/bios

Label-free biosensing of a gene mutation using a silicon nanowire field-effect transistor

Chi-Chang Wu [a], Fu-Hsiang Ko [a,*], Yuh-Shyong Yang [b], Der-Ling Hsia [a], Bo-Syuan Lee [a], Ting-Siang Su [a]

[a] Institute of Nanotechnology, and Department of Materials Science and Engineering, National Chiao Tung University, Hsinchu 300, Taiwan
[b] Department of Biological Science and Technology, National Chiao Tung University, Hsinchu 300, Taiwan

ARTICLE INFO

Article history:
Received 9 June 2009
Received in revised form 3 August 2009
Accepted 21 August 2009
Available online 29 August 2009

Keywords:
Nanowire
Biosensor
Gene mutation sensing
BRAF

ABSTRACT

We have developed a silicon nanowire field-effect transistor (NWFET) that allows deoxyribonucleic acid (DNA) biosensing. The nanowire (NW) was fabricated on a silicon-on-insulator wafer to provide effective ohmic contact. The NWFET sensor displayed n-channel depletion characteristics. To demonstrate the sensing capacity of the NWFET, we employed the $BRAF^{V599E}$ mutation gene, which correlates to the occurrence of cancers, as the target DNA sequence. The threshold voltage of the NWFET increased when the mutation gene was hybridized with the capture DNA strands on the nanowire, and decreased to the original level after de-hybridization of the gene. The shift in the drain current–gate voltage (I_D–V_G) curves revealed that the electrical signal had a logarithmic relationship with respect to the concentration of the mutation gene of up to six orders of magnitude, with the detection limit in the sub-femtomolar level. The detection results of mismatched DNA sequences, including one- and five-base-mismatched DNA strands, could be distinguished from complementary DNA gene by this sensor. The excellent electrical results obtained using this label-free NWFET sensor suggest that such devices might be potentially useful tools for biological research and oncogene screening.

1. Introduction

Ultrasensitive assays for biological and chemical species are fundamental requirements for the screening and detection of disease, as well as for the discovery of new drugs. There is increasing demand for ultrasensitive gene detection systems that allow the early detection of genetic disorders, thereby improving preventative health care. Many of these disorders are caused by in-cell mutations of double-stranded deoxyribonucleic acid (dsDNA), the blueprint of our genetic makeup. Double-stranded DNA comprises pairs of single-stranded DNA (ssDNA) bonded together to form the well-known DNA double helix. Hence, the detection of specific sequences of ssDNA and knowledge of the base pair composition are important aspects of the diagnoses of genetic disorders.

The most widespread technique for assaying DNA samples employs the polymerase chain reaction (PCR) to amplify a DNA fragment or sequence of interest through enzymatic replication (Sano et al., 1992; Tang et al., 2009). PCR has become a common technique in biological and medical research laboratories for such tasks as the sequencing of genes, the detection and diagnoses of infectious diseases, the identification of genetic fingerprints, and the creation of transgenic organisms (Pournaghi-Azar et al., 2008). The drawbacks of such assays include the need for a fluorescent label and the great length of time required to amplify trace DNA concentrations. Higher sensitivity, label-free sensing devices are desired as replacements for the time-consuming, label-based assays (Zhang et al., 2009).

One-dimensional nanowires (NWs; Chen et al., 2006; Hahm and Lieber, 2004; Hsiao et al., 2009; Lee et al., 2009; Lin et al., 2005; Zhang et al., 2009) are particularly appealing candidates for use in ultrasensitive miniaturized biomolecule sensors. Nanowire field-effect transistors (NWFETs) can suppress the short-channel effects encountered in nanoscale metal-oxide semiconductor field-effect transistors and provide high surface sensitivity (Wernersson et al., 2007). Unlike the signal responses of conventional electrochemical cells operate based on the Nernst equation (Rieger, 1987), the response of NWFETs featuring surface-immobilized molecules from the fluid is more complex. Recently, Nair and Alam (2008) derived a logarithmic relationship between the target molecular concentration and the electrical signal for an NWFET functioning based on the diffusion–capture model and the Poisson–Boltzmann equation.

Silicon NWFETs have been fabricated using both “top down” and “bottom up” methods (Lin et al., 2009). The “bottom up” fabrication methods usually involve the formation of NWs through vapor–liquid–solid (VLS) growth (Duan et al., 2003; Hahm and Lieber, 2004), which is limited by the need for complex integra-

* Corresponding author. Tel.: +886 35712121x55803; fax: +886 3 5729912.
E-mail address: fhko@mail.nctu.edu.tw (F.-H. Ko).

0956-5663/$ – see front matter © 2009 Elsevier B.V. All rights reserved.
doi:10.1016/j.bios.2009.08.031

tion techniques that require precise transfer and positioning of individual NWs to provide reliable and superior ohmic contacts. In addition, control over the doping concentrations in self-assembled semiconducting nanostructures remains a great challenge, as is the fabrication of high-density sensor arrays. Furthermore, the use of an additional external gate—to precisely turn the NWFET sensor to higher sensitivity—is also critical (Chen et al., 2006; Hsiao et al., 2009; Li et al., 2004). The "top down" methods for fabricating NWs usually employ the advanced lithography techniques used in the semiconductor industry, allowing mass-production with reduced fabrication costs (Li et al., 2004; Stern et al., 2007a). The excellent device performance and good ohmic contacts of such methods enable the possibility of integration.

It has been reported that the presence of $BRAF^{V599E}$ mutation genes correlates to the occurrence of melanomas, colorectal cancers, gliomas, lung cancers, sarcomas, ovarian carcinomas, breast cancers, papillary thyroid carcinomas, and liver cancers (Davies et al., 2002; Xu et al., 2003). This mutation is believed to mimic phosphorylation in the activation segment by insertion of an acidic residue close to a site of regulated phosphorylation at serine 598. $BRAF^{V599E}$ exhibits elevated basal kinase activity and diminished responsiveness toward oncogenic stimulation. $BRAF^{V599E}$ also transforms NIH3T3 cells (murine embryonic fibroblasts) with higher efficiency than does the wild-type form of the kinase, consistent with the functioning as an oncogene (Kimura et al., 2003). Therefore, characterization of the $BRAF^{V599E}$ mutation genes at the molecular level is significant for early tumor identification, allowing the possibility of aggressive and specific therapy to save human lives.

In this study, we used conventional complementary metal-oxide semiconductor technology to develop a 60-nm-wide Si NWFET that enables the sensing of mutated genes. We first evaluated various cleaning solutions for their use in improving the immobilization of DNA onto the silicon dioxide (SiO_2) surfaces, in terms of the fluorescence efficiency and the electrical properties of the sensors. We then applied the NWFET sensor as an ultrahigh-sensitivity molecular probe for the detection of a cancer-related $BRAF^{V599E}$ mutation gene.

2. Materials and methods

2.1. Fabrication of NWFET sensors

A commercially available 6-in. (100) silicon-on-insulator (SOI) wafer, which possessed 50-nm-thick intrinsic silicon and 150-nm-thick buried oxide, was served as the device substrate (Fig. 1(a)). The detailed fabrication procedures for the back-gated NWFET sensor were mentioned below. The critical silicon NWs having a width of 60 nm and length of 2 μm were defined using a 40-keV electron beam (EB) lithography and dry etching system (Fig. 1(b)). After removal of EB resist, a thin layer of SiO_2 film (10 nm) was then deposited by low-pressure chemical vapor deposition (LPCVD). Again, the EB photoresist (PR) was spin-coated onto the surface. Prior to ion implantation, the PR on the region of defining the source/drain areas was removed by EB lithography. Arsenic ion beam (As^+) was then implanted with a dosage of $5 \times 10^{15}\ cm^{-2}$ at an acceleration energy of 20 keV. Backside of the sample was also boron-implanted at 100 keV with $5 \times 10^{15}\ cm^{-2}$ dosage. After PR removing, rapid thermal annealing (RTA) was performed at 1050 °C for 30 s in a nitrogen ambient to activate the carriers (Fig. 1(c)). Prior to defining the contact pad region through lithography and wet etching (80% phosphoric acid, 5% nitric acid, 5% acetic acid, and 10% de-ionized water; by volume), a 500-nm-thick Al–Si–Cu (Al: 98.5%; Si: 1%; Cu: 0.5%; by weight) alloy was formed using a sputter system (Fig. 1(d)). After PR removal, 50-nm-thick SiO_2 and 10-nm-thick silicon nitride (Si_3N_4) layers were sequentially deposited through plasma-enhanced chemical vapor deposition (PECVD) at 300 °C to passivate the nanowire's surface. Then, the EB lithography was used to open the NWFETs detection region for sensing purpose. The region was sequentially etched back by plasma etch (for Si_3N_4) and diluted buffer oxide etching solution (BOE for SiO_2, NH_4F:HF:de-ionized water = 42:7:1). The PR was then removed by H_2SO_4 and H_2O_2 mixture (3:1; denoted "piranha"), and the schematic diagram was indicated in Fig. 1(e). Then, only the backside surface was dipped and etched by BOE solution in a pipette. Finally, a 500-nm-thick Al–Si–Cu pad was deposited by sputter system. A cross-sectional representation of the NWFET with electrical connection for the detection of DNA molecules is presented in Fig. 1(f). Prior to the DNA immobilization, all the devices were preserved in clean room for at least 1 week to ensure the thickness saturation of native oxide.

2.2. Self-assembly of capture DNA on the NWFET device

Prior to immobilizing the DNA molecules, sensors were cleaned for 30 min using various solutions: (a) no cleaning (denoted "control"), (b) de-ionized water (denoted "DI"), (c) piranha, (d) 25% 2-propanol solution (denoted "IPA"), and (e) acetone and ethanol mixture (1:1; denoted "ACE"). The H_2SO_4, HCl, H_2O_2, and organic

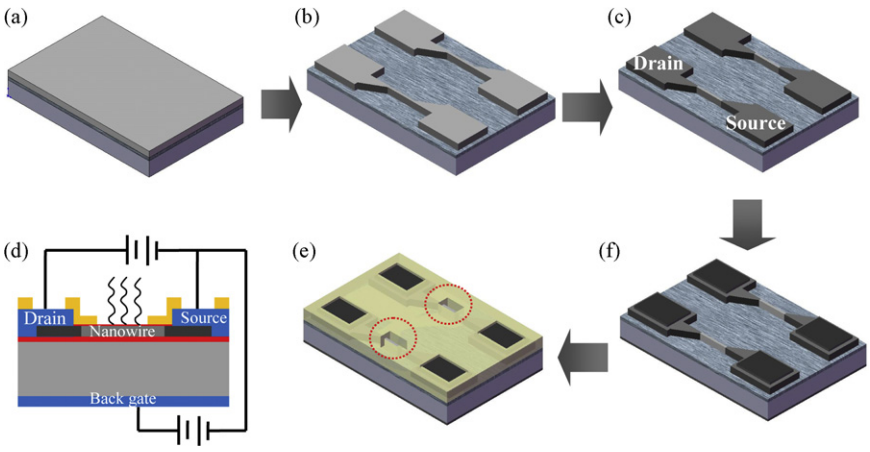

Fig. 1. Schematic representation for the fabrication of the NWFET sensors. (a) A 6-in. SOI wafer (50 nm intrinsic Si; 150 nm buried oxide) was employed as the device substrate. (b) NWs were patterned using an e-beam direct writing and dry etching system. (c) Source/drain implantation and annealing. (d) Contact pad (500 nm Al–Si–Cu film) was deposited at the source/drain region. (e) Passivation layer formed, followed by etching back the detection region for DNA immobilization (red circle). (f) Cross-sectional representation of the completed NWFET sensor and its electrical connection for the detection of DNA strands. (For interpretation of the references to color in this figure legend, the reader is referred to the web version of the article.)

solvents used to clean the device surface were of analytical or higher grade (Merck, Darmstadt, Germany). High-purity DI water, purified through double deionization processes, was used throughout.

After performing the cleaning process, a monolayer of 30-mer ssDNA (capture DNA, Blossom Biotechnologies, Taipei, Taiwan) molecules was then immobilized onto the NWFET surface. The surface reactions occurred with the silanol groups present on the silicon NW surface as a result of silicon oxide formation. Because silanol groups are good proton donors (H^+) and acceptors (SiO^-), (3-aminopropyl)triethoxysilane (APTES) was employed to self-assemble a monolayer of DNA onto the surface of the NW detection region. Fig. 2 illustrates the procedure used to immobilize the DNA strands onto the surface-bounded APTES units. Initially, the samples were immersed into 10% APTES aqueous solution for 30 min at 37 °C and adjusted to pH 3.5 with 1 M HCl. The samples were then rinsed with DI water and dried on a hot plate (120 °C for 30 min). At this stage, amino groups were presented as terminal units from the surface. Next, glutaraldehyde was linked to the amino groups to present aldehyde groups from the surface; the sample was immersed in the linker solution (2.5% glutaraldehyde (1,5-pentanedial)) for 30 min at room temperature and then rinsed with phosphate-buffered saline (PBS; 120 mM NaCl, 2.7 mM KCl, and 10 mM phosphate buffer; pH 7.4; Sigma–Aldrich) solution (Yoshida et al., 1995). The 2.5% glutaraldehyde solution (Stefano et al., 2008; Yakovleva et al., 2002) was formed by diluting 25% glutaraldehyde (Sigma–Aldrich) with PBS solution. Next, the selective immobilization technique was used to bind the terminal 3′-amino group of the oligonucleotide to the aldehyde groups on the NW surface (Turutin et al., 2002). A fresh solution of synthetic 1 μM capture DNA (Blossom Biotechnologies, Taipei, Taiwan) was diluted with PBS buffer to provide a 10 nM solution of capture DNA. A drop (100 μL) of this capture DNA solution was placed onto the NWs and reacted for 1 h to ensure effective immobilization. The un-reacted aldehyde groups were blocked through reactions with ethanolamine (Sigma–Aldrich), washed with PBS buffer, and subsequently dried under ambient nitrogen.

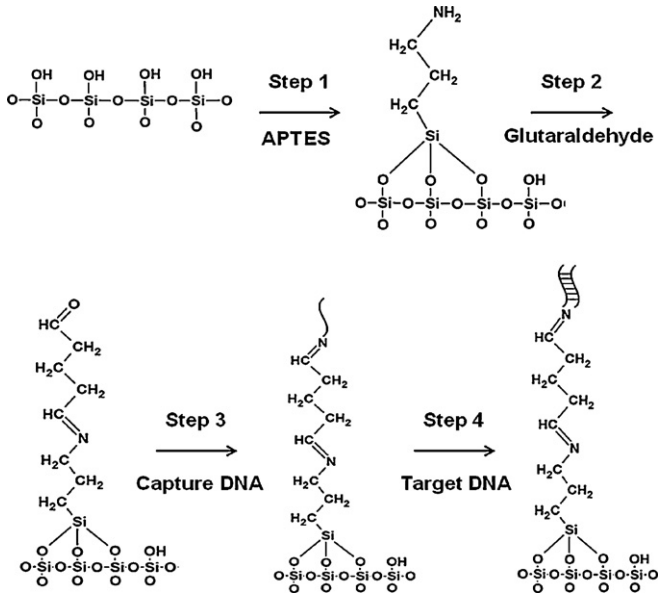

Fig. 2. Self-assembly processes for the immobilization of capture DNA and hybridization of target DNA. (1) The Si NW presenting a native oxide on its surface was coated with APTES. (2) Glutaraldehyde was linked to the amino groups. (3) Terminal 3′-amino groups of the capture DNA strands were reacted with the aldehyde groups. (4) Complementary target DNA was hybridized to the capture DNA on the Si NW surface.

To monitor the efficient immobilization of the capture DNA, a fluorescently labeled capture DNA sample (Blossom Biotechnologies, Taipei, Taiwan) was also prepared. The fluorescent unit was derived from fluorescein isothiocyanate (FITC), which reacted specifically at the 5′ end of the capture DNA. Green fluorescence images (excitation: 494 nm; emission: 520 nm) were observed using a BX51 fluorescence microscope (Olympus, PA, USA).

2.3. Target DNA hybridization and de-hybridization

After capture DNA immobilization, a strand of synthetic complementary DNA, namely the target DNA (Blossom Biotechnologies, Taipei, Taiwan), was applied to hybridize to the capture DNA on the NWFET surface. The sequence of the target DNA was complementary to that of the capture DNA. The 30-mer target DNA was diluted to various concentrations with PBS buffer solution. The target DNA was then injected into the microfluidic channel that ran through the NWFET detection region, followed by PBS washing to remove the excess target DNA. The electrical measurement of the NWFET sensor was performed to obtain the drain current (I_D) versus gate voltage (V_G) curve. To ensure successful hybridization, an FITC-labeled target DNA strand, with the fluorescent unit located at the 3′ end, was also prepared.

The electrical properties of the NWFET biosensors were characterized using an Agilent-4156C semiconductor parameter analyzer (Agilent Technologies, CA). After measurement, the samples were washed with hot DI water (90 °C) for 5 min to de-hybridize the complementary DNA pair. The resulting surface presenting only the capture DNA was then measured again.

3. Results and discussion

3.1. Electrical performance of the NWFET

Fig. 3 presents plot of the I_D–V_G at drain voltages (V_D) of 0.1 and 1 V, respectively, for the fabricated 60-nm NWFET biosensor. The current flowing through the NW located between the source and drain electrodes could be switched “on” and “off” at various backside gate potentials. If, at a large negative gate bias (e.g., −15 V), the channel conduction (I_D) is very low, a positive voltage applied to the gate will create an n-channel (i.e., an electron carrier). Therefore, the sensor is a normally-on, n-channel depletion NWFET (Sze, 1981). In general, a backside gate can apply a bias voltage to the NW and, thereby, affect the energy barrier for the charge carriers. This applied voltage ensures device operation under the

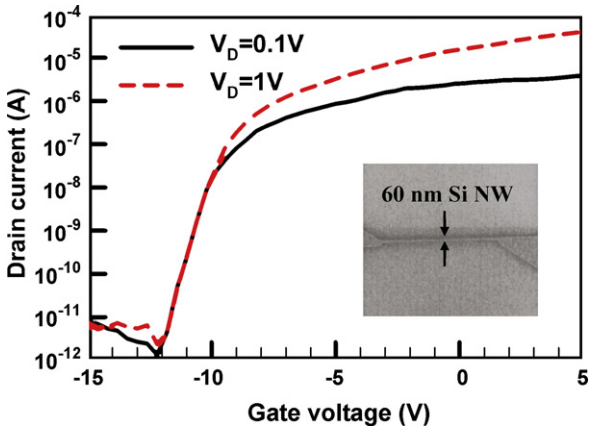

Fig. 3. Plots of drain current versus gate voltage for the NWFET sensor, measured at values of V_D of 0.1 (black line) and 1 V (red dotted line). Inset: scanning electron microscopy image of the 60 nm-wide Si NW. (For interpretation of the references to color in this figure legend, the reader is referred to the web version of the article.)

optimal conditions of a larger current shift. Stern et al. (2007b) proposed a p-channel DNA sensor with a backside gate control design; the sub-threshold swing (SS) for their device was, however, about 1250 mV/decade ($I_D = 10^{-13}$ and 10^{-9} A at −20 and −25 V, respectively)—much higher than our value of 450 mV/decade. We attribute the high sensitivity of our DNA sensor to the use of the single crystal n-channel design rule having higher mobility and lower SS characteristic.

The turn-on/turn-off current ratio of this sensor was near six orders of magnitude when V_D was 0.1 V, suggesting improved practicality of the fabricated biosensors. The threshold voltage (V_t), which we determined for a drain current at 10^{-9} A, was ca. −10.8 V. The dependence of the value of I_D on the applied gate voltage implies that the fabricated NWFET sensors could be fine-tuned to optimal conditions to sense molecules that effect a change in the surface charge. A charged molecule bound onto an NW surface exerts an electric field in a manner similar to an applied gate voltage. For example, when the surface receptor contains a macromolecule of DNA bearing negative charge, specific binding interactions will result in an increase in the NW's negative charge, and, hence, a shift to the right for the V_t in I_D–V_G curve of the NWFET biosensor (Lin et al., 2009).

3.2. Evaluating of cleaning efficiency through fluorescence imaging

The charge carriers in the NWs are affected by the presence of the immobilized biomolecule; therefore, the variation of their electrical signal can be used as the sensing indicator. If the surface of interest is covered by ambient contaminants, the detection region of the NW is blocked by the contaminants, which degrade the function of the sensor. Conventional bioassays described in the literature have been cleaned using piranha solution (Bras et al., 2004; Volle et al., 2003), even though it is not appropriate for sensor cleaning when the technology advances to the bio-electronic era. For example, piranha solution would corrode all of the metal contacts, e.g., the Al–Si–Cu alloys that are the most commonly used in semiconductor manufacturing. Hence, we sought a relative mild cleaning method that would restore the electrical signal in the NW devices—one that could be used as a substitute for washing with piranha solution—in the blooming field of coupling biomolecules to semiconductor electronics.

A silicon substrate on which stacked with $SiO_2/Si_3N_4/SiO_2$ film in a low-pressure quartz furnace was employed to test the efficiency of the various cleaning solutions. The primary SiO_2 film was a buffer layer to prevent the Si_3N_4 film from peeling off. The upper SiO_2 film was then patterned to form a line structure, as indicated in Fig. 4(a). The content of cleaning solutions and the post-cleaning immobilization procedure were mentioned in Section 2.2. Because the immobilization efficiency of DNA on a SiO_2 surface is much higher than that on Si_3N_4, the immobilization selectivity of DNA on these materials could be distinguished by using the line structure. Prior to immobilizing the 10 nM FITC-labeled capture DNA, the 1-day ambient exposure samples were subjected to cleaning with various solutions to test their cleaning efficiencies. The intensity of fluorescence signal on the SiO_2 surface was then characterized to evaluate the cleaning efficiency. Quantification of the fluorescence images was achieved by the software of Image-Pro Plus (Media cybernetic®). Fig. 4(b) displays fluorescence images of the samples without cleaning (control) and after cleaning with DI, piranha, IPA, and ACE. The intensities of fluorescence signal for control and the samples cleaned using DI, piranha, IPA, and ACE are 4.2 ± 0.2, 7.4 ± 0.3, 45.8 ± 1.5, 21.5 ± 0.9, and 33.5 ± 1.4, respectively. Obviously, the samples cleaned using piranha and ACE displayed clear fluorescence images, suggesting that these two solutions were effective surface cleaning agents. Moreover, the fluorescence appeared only on the SiO_2 patterns, indicated that DNA immobilization was unfavorable on the Si_3N_4 surfaces. In contrast, the weak fluorescence images of the surfaces washed with either DI or IPA indicate that they were not cleaned effectively; i.e., the contaminants remaining on the surface affected the immobilization of DNA. Despite its superior cleaning efficiency, piranha solution is very reactive and will corrode interconnect metals. The mild ACE cleaning solution appears to be a good substitute for the traditional piranha solution when cleaning NWFET biosensors.

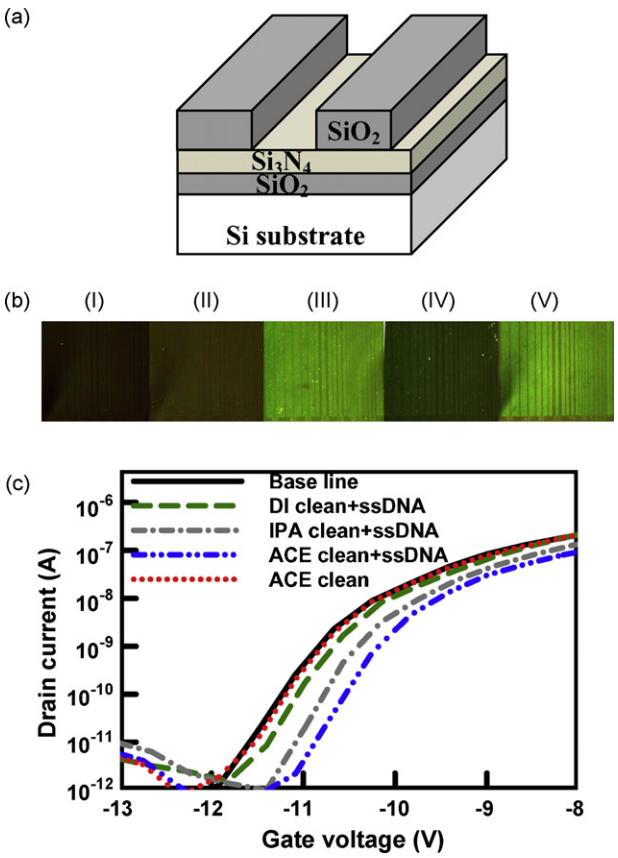

Fig. 4. (a) Schematic representation of the SiO_2 line structure used to test the immobilization efficiency. The underlying Si_3N_4 film was used to define the selectivity, because of the higher DNA immobilization efficiency of SiO_2 relative to that of the Si_3N_4 surface. (b) Fluorescence images of the (I) uncleaned (control) sample and (II–V) the samples cleaned with (II) DI, (III) piranha, (IV) IPA, and (V) ACE. (c) Electrical responses of the NWFET sensor with capture DNA immobilized after using various cleaning methods. The I_D–V_G curves were recorded at a constant drain voltage ($V_D = 0.1$ V). The base line curve was recorded for the sample prior to cleaning but after treatment with PBS (black line). Curves were recorded for the DNA-immobilized NWFET sensors after washing with DI (green dotted line), IPA (gray dotted line), and ACE (blue dotted line). The curve recorded for the sample after ACE cleaning but without DNA immobilization (red dotted line) was recorded to confirm the influence of the cleaning process. (For interpretation of the references to color in this figure legend, the reader is referred to the web version of the article.)

We also characterized the immobilization efficiency in terms of the electrical properties of the NWFET biosensors. Fig. 4(c) illustrates the I_D–V_G curves recorded at a constant drain voltage ($V_D = 0.1$ V) for various resulting NWFET sensors. The threshold voltage of the base line (prior to cleaning and immobilization of capture DNA) was −10.80 V. It appears that the surfaces washed with DI and IPA was not cleaned effectively; only a few DNA strands bound to the NW, causing small rightward shifts of the threshold voltage (0.15 and 0.42 V, respectively). In contrast, surface cleaning was effective when using the ACE mixture (rightward shift of 0.63 V for the curve); this clean surface allowed more DNA strands to self-assemble, consistent with the fluorescence images in Fig. 4(b). To clarify the influence of the ACE cleaning process, we also measured

the electrical properties of the sample after ACE cleaning but without DNA immobilization. In this case, the I_D–V_G curve was almost identical to that of the sample prior to cleaning, implying that the threshold voltage shift arose mainly as a result of immobilizing the DNA strands on the NW surface.

3.3. Using the NWFET to detect a mutated gene

To detect BRAF^{V599E} mutation genes, we cleaned the surface of the NWFET with ACE and then immobilized a 30-mer capture DNA strand, having the sequence 5′-AAATATATTA-TTACTCTTGA-GGTCTCTGTG-3′, onto the surface. This capture DNA sequence is fully complementary to that of the target DNA which is partial sequence of the BRAF^{V599E} mutation gene (Liao et al., 2009). Hence, the capture DNA on the NW surface formed a molecular probe for the detection of target DNA having the specific gene sequence 5′-CACAGAGACC-TCAAGAGTAA-TAATATATTT-3′. Fig. 5(a) reveals the ability of the NWFET biosensors to detect cancer-related mutation genes. The threshold voltage for the capture DNA-modified NWFET, measured in PBS buffer solution, was −10.16 V (base line). Various concentrations of the target DNA, containing the BRAF^{V599E} mutation gene, were adsorbed onto the surface of the NWFET device, providing a further rightward shift of the I_D–V_G curve, indicating the successful hybridization of the complementary mutation gene with the capture DNA. The fluorescence image in inset (I) confirms the successful hybridization of the 10 nM FITC-labeled target DNA to the capture DNA.

For de-hybridization, we washed this dsDNA sample with hot DI (90 °C) to separate the target DNA from the probe surface; the curve returned to almost the same level as that of the base line. To ensure de-hybridization, we also used the FITC-labeled DNA to trace the reaction pathway of the molecule of interest on the surface. The fluorescence image of the sample obtained after de-hybridization of the FITC-labeled target DNA [inset (II)] reveals that the target DNA was completely separated from the NW surface after de-hybridization.

Fig. 5(b) reveals the exponential relationship between the voltage shift of the NWFET sensor and the target DNA concentration. The voltage shift for the NWFET sensor under various target DNA concentrations of 10 fM, 1 pM, 100 pM, and 10 nM was 0.22 ± 0.03, 0.45 ± 0.05, 0.69 ± 0.04, and 0.81 ± 0.04 V, respectively. The relationship between the response of a nanobiosensor and the DNA concentration has been reported previously (Nair and Alam, 2008) to be

$$S(t) \propto \ln[\rho_0]$$

where $S(t)$ is the sensor response, which is either a voltage or current shift, and $[\rho_0]$ is the DNA concentration. This equation suggests that the response of a nanoscale sensor should exhibit a logarithmic dependence on the DNA concentration, consistent with our finding. The linear fitting for the calibration curve is $y = 0.119 \times \log(x) + 1.8817$ from 10 fM to 100 pM with correlation coefficient of 0.988. The detection limit, which is defined as the minimal mutation gene concentration that gives a voltage shift which is three times the standard deviation, is estimated to 0.88 fM from the calibration curve. In addition, the relative standard deviation of threshold voltage shift for the target DNA is less than 12%.

Fig. 6 reveals the specific detection of target DNA using our NWFET. We investigated the behavior of mismatched target DNA strands (concentration: 10 nM) containing one and five mismatched bases; their DNA sequences were 5′-CACAGAGACC-TCAAGTGTAA-TAATATATTT-3′ and 5′-CACAGAGACC-TCAAG-TACGG-TAATATATTT-3′, respectively. The latter exhibited the same response as that of the base line, whereas the former exhibited a rightward shift but could still be distinguished from the

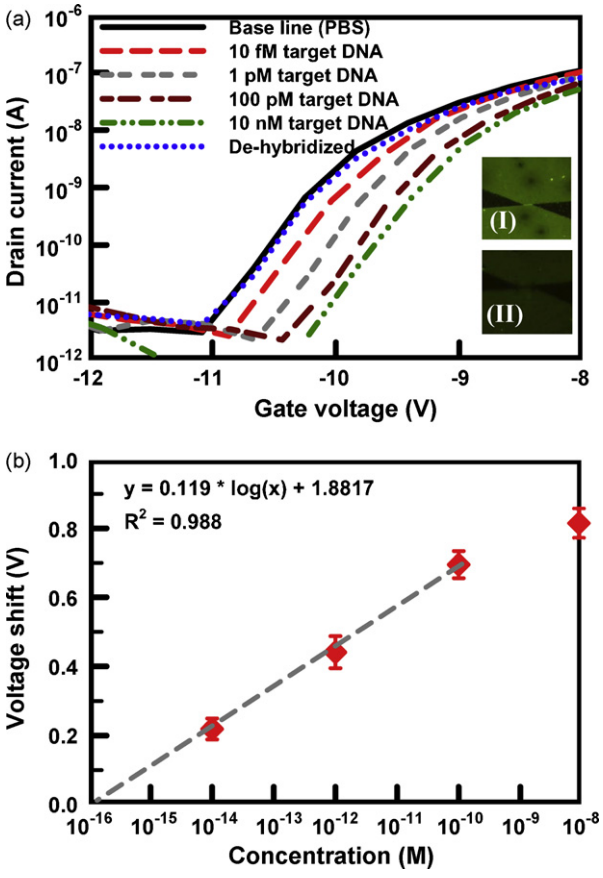

Fig. 5. (a) Concentration-dependent electrical response of the capture DNA-modified NWFET sensor when detecting target DNA. The I_D–V_G curve of the base line was obtained in PBS buffer (black line); PBS buffer solutions containing target DNA at various concentrations (10 fM, 1 pM, 100 pM, 10 nM) were injected, respectively, and the I_D–V_G curves recorded. The de-hybridized samples were obtained after treatment of the dsDNA with hot DI water (90 °C); the I_D–V_G curves were then measured (red dotted line). Inset (I): fluorescence image of 10 nM FITC-labeled target DNA bound to the capture DNA. Inset (II): fluorescence image of the FITC-labeled target DNA after de-hybridization. (b) Voltage shift (from $n = 4$) of the NWFET sensor plotted with respect to the target DNA concentration. The voltage shift was extracted from (a) at a constant drain current (I_D = 1 nA). (For interpretation of the references to color in this figure legend, the reader is referred to the web version of the article.)

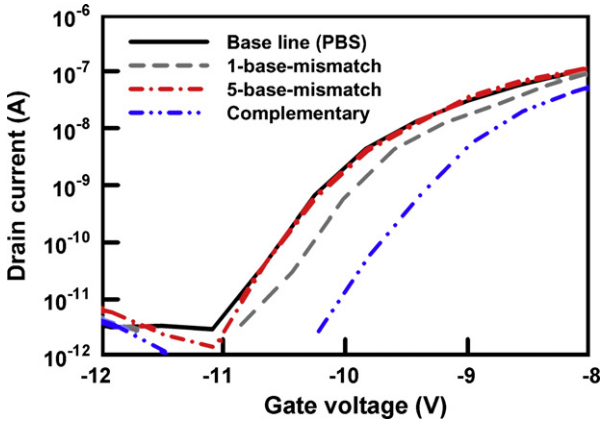

Fig. 6. Electrical response of the capture DNA-modified NWFET sensor when detecting mismatched target DNA. The I_D–V_G curve of the base line was recorded in PBS buffer (black line); PBS buffer solution containing one- or five-base-mismatched target DNA strands (10 nM) was injected and the I_D–V_G curves were recorded. (For interpretation of the references to color in this figure legend, the reader is referred to the web version of the article.)

complementary sample. These results suggest that the single-base-mismatched target DNA hybridized to a small degree, but the five-base-mismatched DNA barely reacted with the capture DNA. A similar result has been reported for three-base-mismatched mutant genes, which interacted nonspecifically with an NW sensor, but could be quantified and distinguished from their corresponding wild-type genes (Hahm and Lieber, 2004).

4. Conclusions

Using a cleaning solution prepared from a mixture of acetone and ethanol allowed us to develop an NWFET device that behaved as a biomolecular sensor for an oncogene. We used the state-of-the-art semiconductor line to fabricate label-free NWFET devices having line widths of 60 nm. Connecting the NWs to source and drain electrodes fabricated on the SOI wafer provided functioning ohmic contacts without the problem of contact resistance. The NWFET exhibited n-channel depletion characteristics that allowed detection of the hybridization and de-hybridization of a $BRAF^{V599E}$ mutation gene from a cancer cell, as well as the ability to distinguish between complementary and mismatched target DNA. The detection limit of the NWFET biosensor for the sensing of the mutation gene was in the sub-femtomolar regime. Because this label-free NWFET sensor displayed the ability to detect the oncogene, such devices are potentially useful tools for biological research and genetic screening.

References

Bras, M., Dugas, V., Bessueille, F., Cloarec, J.P., Martin, J.R., Cabrera, M., Chauvet, J.P., Souteyrand, E., Garrigues, M., 2004. Biosens. Bioelectron. 20, 797–806.

Chen, Y., Wang, X., Erramilli, S., Mohanty, P., Kalinowski, A., 2006. Appl. Phys. Lett. 89, 223512.

Davies, H., Bignell, G.R., Cox, C., Stephens, P., Edkins, S., Clegg, S., Teague, J., Woffendin, H., Garnett, M.J., Bottomley, W., Davis, N., Dicks, E., Ewing, R., Floyd, Y., Gray, K., Hall, S., Hawes, R., Hughes, J., Kosmidou, V., Menzies, A., Mould, C., Parker, A., Stevens, C., Watt, S., Hooper, S., Wilson, R., Jayatilake, H., Gusterson, B.A., Cooper, C., Shipley, J., Hargrave, D., Pritchard-Jones, K., Maitland, N., Chenevix-Trench, G., Riggins, G.J., Bigner, D.D., Palmieri, G., Cossu, A., Flanagan, A., Nicholson, A., Ho, J.W.C., Leung, S.Y., Yuen, S.T., Weber, B.L., Seigler, H.F., Darrow, T.L., Paterson, H., Marails, R., Marshall, C.J., Wooster, R., Stratton, M.R., Futreal, P.A., 2002. Nature 417, 949–954.

Duan, X., Niu, C., Sahi, V., Chen, J., Parce, J.W., Empedocles, S., Goldman, J.L., 2003. Nature 425, 274–278.

Hahm, J., Lieber, C.M., 2004. Nano Lett. 4, 51–54.

Hsiao, C.Y., Lin, C.H., Hung, C.H., Su, C.J., Lo, Y.R., Lee, C.C., Lin, H.C., Ko, F.H., Huang, T.Y., Yang, Y.S., 2009. Biosens. Bioelectron. 24, 1223–1229.

Kimura, E.T., Nikiforova, M.N., Zhu, Z., Knauf, J.A., Nikiforov, Y.E., Fagin, J.A., 2003. Cancer Res. 63, 1454–1457.

Lee, H.-S., Kim, K.S., Kim, C.-J., Hahn, S.K., Jo, M.-H., 2009. Biosens. Bioelectron. 24, 1801–1805.

Li, Z., Chen, Y., Li, X., Kamins, T.I., Nauka, K., Williams, R.S., 2004. Nano Lett. 4, 245–247.

Liao, K.-T., Cheng, J.-T., Li, C.-L., Liu, R.-T., Huang, H.-J., 2009. Biosens. Bioelectron. 24, 1899–1904.

Lin, H.C., Lee, M.H., Su, C.J., Huang, T.Y., Lee, C.C., Yang, Y.S., 2005. IEEE Electron Device Lett. 26, 643–644.

Lin, C.-H., Hung, C.-H., Hsiao, C.-Y., Lin, H.C., Ko, F.-H., Yang, Y.-S., 2009. Biosens. Bioelectron. 24, 3019–3024.

Nair, P.R., Alam, M.A., 2008. Nano Lett. 8, 1281–1285.

Pournaghi-Azar, M.H., Alipour, E., Zununi, S., Froohandeh, H., Hejazi, M.S., 2008. Biosens. Bioelectron. 24, 524–530.

Rieger, P.H., 1987. Electrochemistry. Prentice-Hall, New Jersey, pp. 12–15.

Sano, T., Smith, C.L., Cantor, C.R., 1992. Science 258, 120–122.

Stefano, L.D., Vitale, A., Rea, I., Staiano, M., Rotiroti, L., Labella, T., Rendina, I., Aurilia, V., Rossi, M., D'Auria, A., 2008. Extremophiles 12, 69–73.

Stern, E., Klemic, J.F., Routenberg, D.A., Wyrembak, P.N., Turner-Evans, D.B., Hamilton, A.D., LaVan, D.A., Fahmy, T.M., Reed, M.A., 2007a. Nature 445, 519–522.

Stern, E., Wagner, R., Sigworth, F.J., Breaker, R., Fahmy, T.M., Reed, M.A., 2007b. Nano Lett. 7, 3405–3409.

Sze, S.M., 1981. Physics of Semiconductor Devices, 2nd edition. John Wiley & Sons, New York, pp. 454–456.

Tang, L., Zeng, G., Shen, G., Li, Y., Liu, C., Li, Z., Luo, J., Fan, C., Yang, C., 2009. Biosens. Bioelectron. 24, 1474–1479.

Turutin, D.V., Zatsepin, T.S., Timchenko, M.A., Kubareva, E.A., Oretskaya, T.S., 2002. Mol. Biol. 36, 705–707.

Volle, J.-N., Chambon, G., Sayah, A., Reymond, C., Fasel, N., Gijs, M.A.M., 2003. Biosens. Bioelectron. 19, 457–464.

Wernersson, L.-E., Lind, E., Samuelson, L., Lowgren, T., Ohlsson, J., 2007. Jpn. J. Appl. Phys. 46, 2629–2631.

Xu, X., Quiros, R.M., Gattuso, P., Ain, K.B., Prinz, R.A., 2003. Cancer Res. 63, 4561–4567.

Yakovleva, J., Davidsson, R., Lobanova, A., Bengtsson, M., Eremin, S., Laurell, T., Emneus, J., 2002. Anal. Chem. 74, 2994–3004.

Yoshida, S., Kanno, H., Watanabe, T., 1995. Anal. Sci. 11, 251–256.

Zhang, G.J., Chua, J.H., Chee, R.-E., Agarwal, A., Wong, S.M., 2009. Biosens. Bioelectron. 24, 2504–2508.